Experimental investigation on the effects of the standoff distance and the initial radius on the dynamics of a single bubble near a rigid wall in an ultrasonic field

Hao Wu[a], Cheng Zhou[b], Zhihua Pu[a], Xiaochen Lai[a], Haixia Yu[b], Dachao Li[a],*

[a] State Key Laboratory of Precision Measuring Technology and Instruments, Tianjin University, Tianjin 300072, PR China
[b] Tianjin Key Laboratory of Biomedical Detecting Techniques and Instruments, Tianjin University, Tianjin 300072, PR China

ARTICLE INFO

ABSTRACT

Bubble behaviors near a boundary in an ultrasonic field are the fundamental forms of acoustic cavitation and of substantial importance in various applications, such as industry cleaning, chemical engineering and food processing. The effects of two important factors that strongly affect the dynamics of a single acoustic cavitation bubble, namely, the initial bubble radius and the standoff distance, were investigated in this work. The temporal evolution of the bubble was recorded using high speed microphotography. Meanwhile, the time of bubble collapse and the characteristics of the liquid jets were analyzed. The results demonstrate that the intensity of the acoustic cavitation, which is characterized by the time of bubble collapse and the liquid jet speed, reaches the optimum level under suitable values of the initial bubble radius and the normalized standoff distance. As the initial bubble radius and the normalized standoff distance increase or decrease from the optimal values, the time of the bubble collapse increases, and the first liquid jet's speed decreases substantially, whereas the speeds of the second and third liquid jets exhibit no substantial changes. These results on bubble dynamics in an ultrasonic field are important for identifying or correcting the mechanisms of acoustic cavitation and for facilitating its optimization and application.

1. Introduction

Acoustic cavitation has been applied in many fields, such as ultrasound cleaning [1,2], water filtration [3] and food processing [4]. To investigate the potential mechanisms that underlying surface cleaning, erosion and sonoporation, which would facilitate optimization or extend the applications, experiments have been conducted [5–10]. It is concluded that the strong boundary layer flows of liquid, the capillary forces and the pressure shocks from bubble collapse and jet impact at solids can help to remove particles from the surface in surface cleaning system [2]. The high-speed liquid jet is also regarded as the main contributor to the high pressure on the nearby boundary in the application of destructive erosion [11,12]. In all applications of acoustic cavitation, the dynamic behaviors of microbubbles around the rigid boundary are directly related to its efficiency and are strongly influenced by each bubble's initial radius and standoff distance. However, due to the randomness of the bubble size and bubble distribution in the ultrasonic field, the exact influence mechanisms have not been identified.

Bubble dynamics in an ultrasonic field is a typical example of multiphase fluidics. During the vibration of an acoustic wave, a bubble becomes shape-unstable and collapses. As the rapid process of bubble collapse is difficult to record experimentally, many numerical simulations have been conducted [13–23] to investigate the mechanism of single bubble dynamics in an ultrasonic field. Osterman et al. [19] and Liu et al. [16] attempted to directly solve the continuity and the Navier-Stokes equations in orthogonal curvilinear coordinates via the volume of fluid (VOF) method and the boundary-fitted finite-volume method (FVM), respectively. They found that the surface tension suppresses the development of non-spherical shape modes for small single bubble; however, the accuracies of these methods are limited by the resolution of the generated mesh. Chahine et al. [24] and Curtiss et al. [6] applied the boundary element method (BEM) to successfully simulate the dynamics of acoustic bubbles without considering the compressibility or viscosity of the liquid. Afterwards, the viscosity and surface tension were analyzed in a simulation of acoustic bubbles via the coupled level-set and volume-of-fluid (CLSVOF) method by Wang et al. [25]. This method has higher accuracy; however, the calculation process is
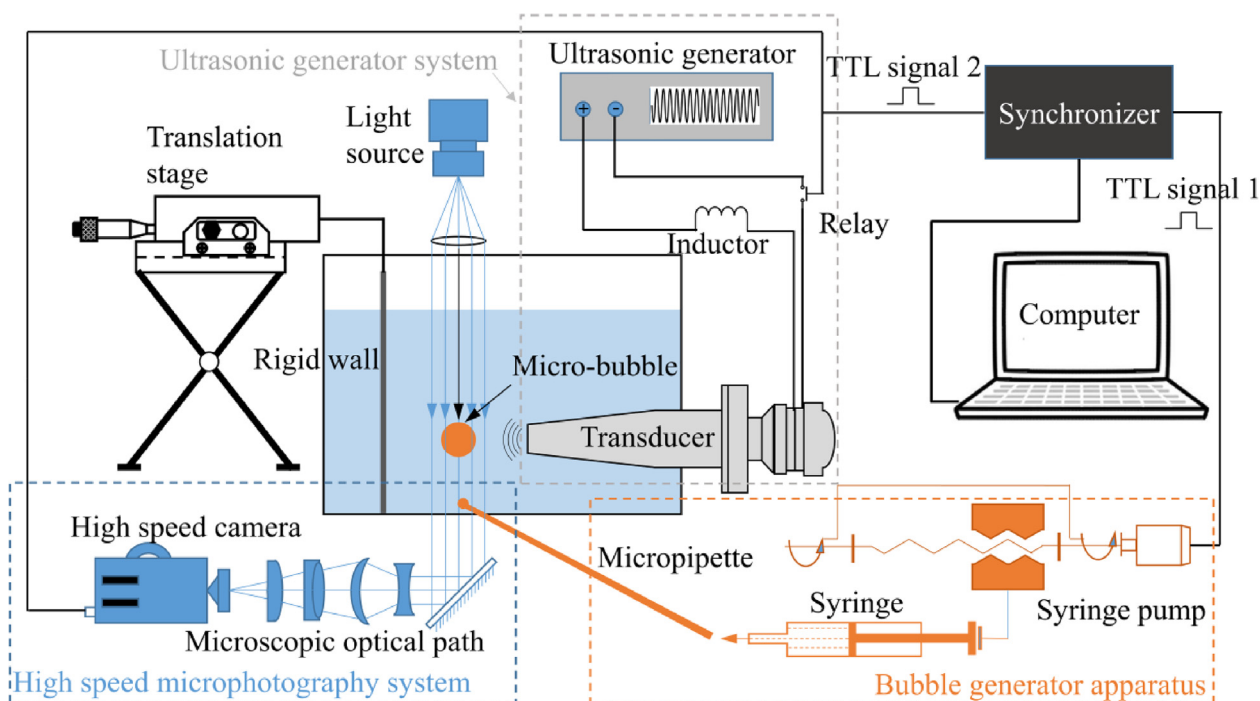

Fig. 1. A schematic of the experimental system.

complex and requires more time. In addition, Wang and Blake [26,27] applied the mixed Palerian-Lagrangian and modified boundary integral method in the simulation of acoustic cavitation. The compressibility and viscosity are considered in these works, and the efficiency of this method is very high.

Due to the small size of an acoustic cavitation bubble and the rapid process of the collapse, experiments are difficult to conduct and are rarely reported. Early experimental studies on single bubble dynamics in an ultrasonic field were reported in the works of Ohl et al. [28], Leighton [29], and Blake et al. [30]. Ohl et al. [28] attempted to generate a single bubble in a container via electrolysis, and applied ultrasound to investigate the bubble's dynamic behaviors in the field. The Bjerknes force was found to be an important factor that influences the interaction between a single bubble and the sound wave. Due to the differences in bubble formation mechanism between electrolysis and acoustic cavitation, the surface tension coefficient and the content of the bubble may both differ, which could influence the bubble's dynamics. Ma et al. [7] investigated the dynamics of a gas bubble that was generated by an injection syringe. Since the bubble was too large (larger than 2 mm), the buoyance not only influenced the shape of the bubble but also substantially affected its dynamics in an ultrasonic field. Therefore, Vyas and Dehghani et al. [31] directly investigated individual cavitation bubble in micrometer size around ultrasonic scalers using high speed recordings up to a million frames per second. In this work, the bubble speed increased over its oscillation cycle and a maximum speed of 27 m/s was recorded during the collapse phase. However, neither the sizes nor the positions of the generated bubbles could be controlled.

Various conditions in acoustic cavitation strongly affect the intensity and would further affect the application efficiency, such as the cleaning efficiency [2] and food production efficiency [4]. To investigate the related mechanisms, studies on how initial conditions (including boundary, ultrasonic field and bubble conditions) affect the dynamics of a bubble in an ultrasonic field have been conducted [32,33]. Kim et al. [34] employed high speed photography to investigate the single bubble behaviors near the wall of a microstructure. They found that the bubble's size and acoustic pressure strongly affected the bubble's dynamics in the ultrasonic field. However, no

detailed analysis was conducted on the bubble dynamics, which could influence the pressure on the wall. Versluis et al. [8] emphatically investigated the shape oscillation of a bubble in an ultrasound field with various ultrasonic frequencies using a high-speed camera. They found that a moving micro bubble not only oscillates in radius but also exhibits asymmetric shape oscillations. Lauterborn et al. [35] and Brujan [36] studied the bubble dynamics under various bubble initial conditions and found that bubbles that differ in terms of their normalized initial standoff distances typically exhibit different dynamics. However, they only focus on the differences in the bubbles' shape changes; no further analysis of the bubbles' important characteristics was conducted due to the limited temporal and spatial resolutions. Wu et al. [37] investigated the dynamics of a bubble near a rigid wall in an ultrasonic field. They found that the bubble would oscillate, move to the rigid wall, collapse and rebound under the excitation of ultrasound and the dynamics of the bubble after its rebound phase were substantially influenced by the intensity of the ultrasonic field. However, other important factors, such as the initial size and standoff distance of the bubble, were not discussed. Up to present, due to the difficulty of controlling the bubble's size and its relative position in the ultrasonic field, how the initial size of an individual acoustic cavitation bubble affects its characteristics near a rigid wall has not been experimentally investigated under various standoff distances.

In the present work, a gas bubble with a controllable initial radius and standoff distance to the rigid wall was generated in a liquid, and the temporal evolution of the bubble with various initial radii and normalized standoff distances in an ultrasonic field was recorded via synchronous high speed microphotography. In addition, the time of bubble collapse and the characteristics of the high-speed jets that were emitted during bubble collapse were quantified and analyzed under various initial conditions. Finally, potential mechanisms by which the initial conditions affect the acoustic cavitation were investigated via experimental methods.

2. Experimental setup

To study the effect of the standoff distance and initial radius on acoustic cavitation bubble dynamics at the microscale level, a bubble
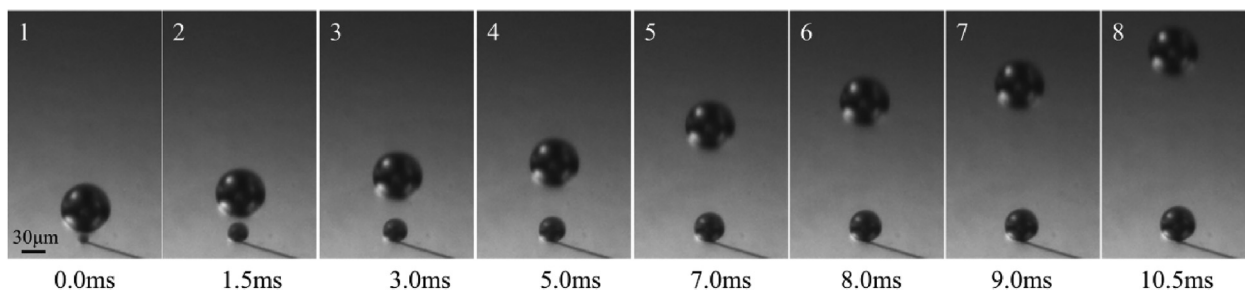
Fig. 2. Temporal evolution of a bubble that is rising in a quiescent liquid without any acoustic waves. The bubble radius is $R_0 = 30$ μm and the recording rate is 2000 fps.
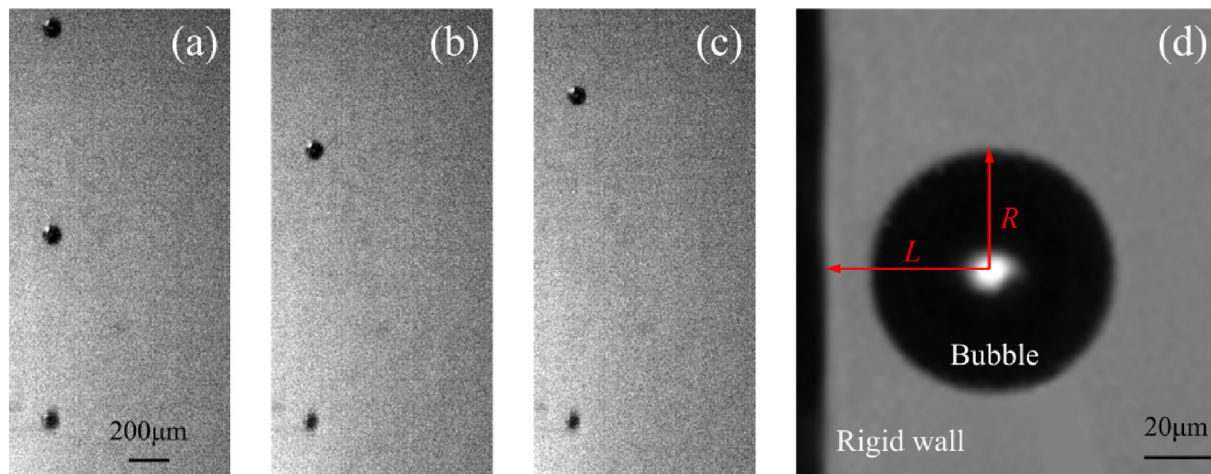

Fig. 3. Generation of a train of bubbles in a liquid under the following flow speeds: (a) 1 ml/min, (b) 2 ml/min and (c) 3 ml/min; (d) detailed information about the position of the bubble relative to the rigid wall.
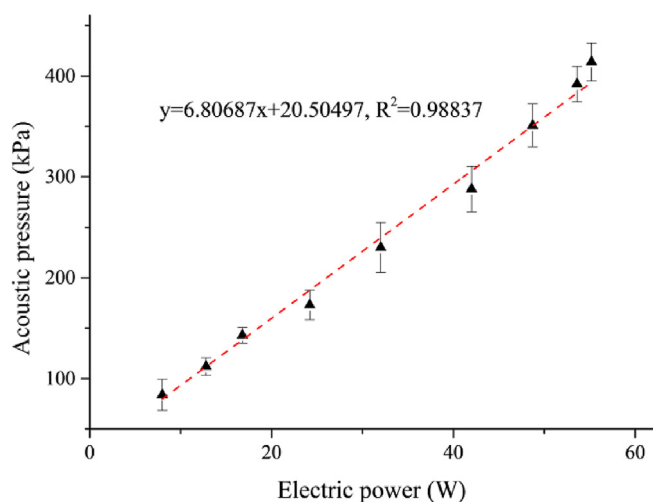

Fig. 4. Plot of the measured electric power and the corresponding acoustic pressure at a distance of 1 cm to the transducer surface.

generator apparatus, an ultrasonic generator system and a high speed microphotography system are needed, as illustrated in Fig. 1, these three parts are contained in orange, gray and blue dotted frame respectively. The experiments in this work were conducted in a cuboid-shaped acrylic glass box (40 mm height and 100 mm length and width), which contained sufficient degassed water. The temperature of the water was maintained at 20 °C.

Single air bubbles with radii that range from 15 to 40 μm were generated in a regulated co-flow micropipette injector, as described by Palanchon et al. [38]. The initial radius of the bubble and the

separation distance are mainly determined by the size of the micropipette's tip and the flow speed. For a micropipette tip diameter of 3 μm, an example of a generated bubble is shown in Fig. 2 under the flow speed of 1 ml/min. The generated bubble has an initial radius of approximately 30 μm. As the bubble rises in the water, its shape remains spherical with no readily observed change in the size. According to Fig. 3, the bubbles with different sizes would generate under various flow speeds, which could be used to control the initial sizes of the generated bubbles. In addition, the distance between two adjacent bubbles is relatively large (larger than 800 μm); hence, the bubbles do not influence each other. To control the gas bubbles at various positions relative to the solid wall, the location of the rigid wall can be changed via a translation stage, as illustrated in Fig. 1. The normalized standoff distance between the bubble and the rigid wall can be calculated via the formula $\gamma = L/R_0$, where L is the distance from the bubble center to the wall at inception and R_0 is the initial radius of the generated bubble, as shown in Fig. 3(d).

Acoustic waves were generated by an acoustic transducer with a resonant frequency of 20.47 kHz. The electrical input power of the acoustic transducer was provided by a commercial high-power ultrasonic generator. In addition, an inductor of 330 μH was used to realize the impedance matching and a relay was connected to the circuit as an electric control toggle switch for synchronous control, as shown in Fig. 1. To correlate the electrical power and the acoustic pressure, the acoustic pressure was measured with a hydrophone (TC4013, RESON, Denmark) that was positioned 1 cm in front of the transducer surface in the water where the bubble was generated and caught, and the electric power was monitored by sampling the voltage and current of the ultrasonic generator. Fig. 4 plots the relationship between the electric power and the acoustic pressure, and the error bars show the good consistency of the measurement results. In the present work, the electric
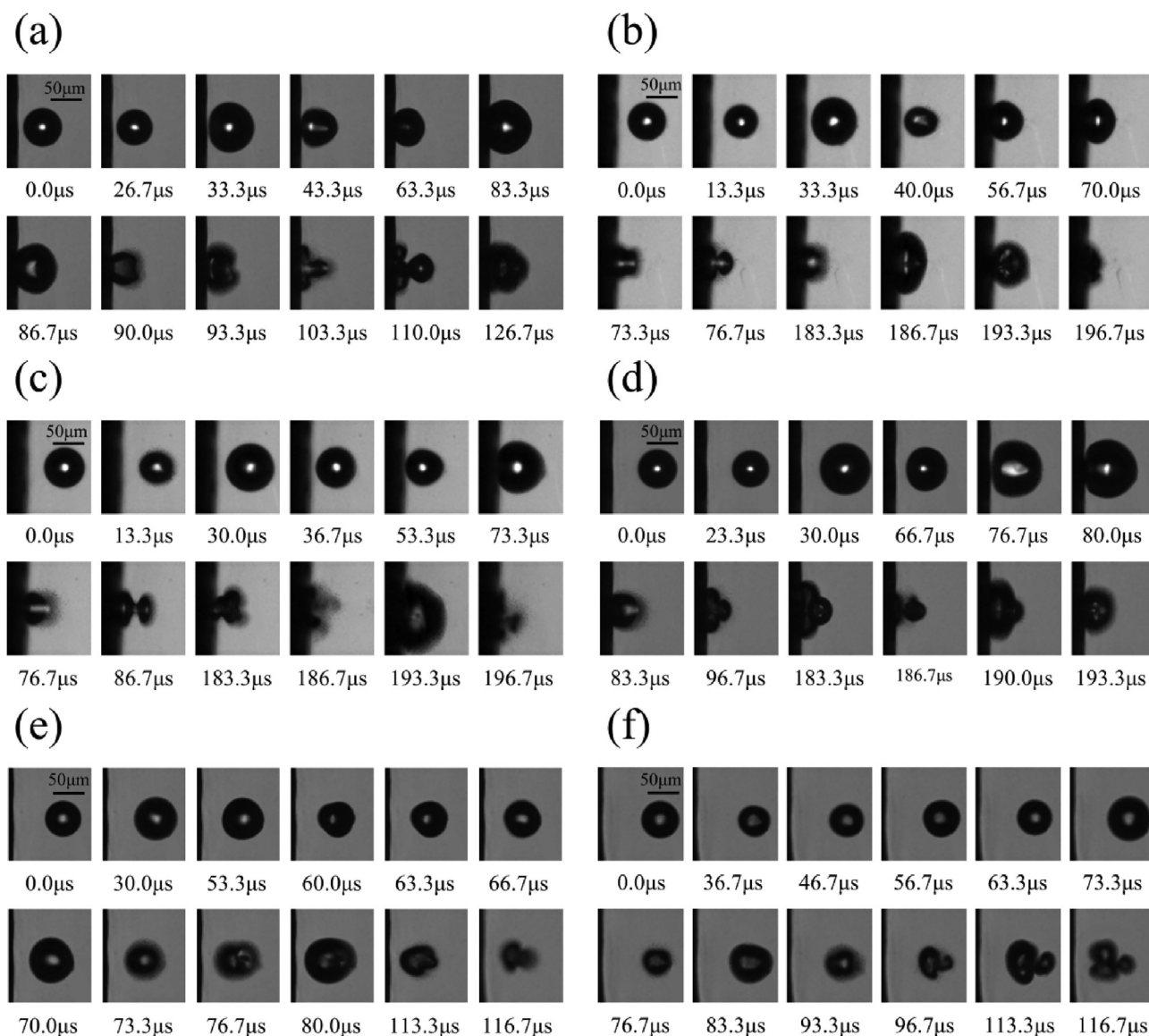
Fig. 5. Temporal evolution of individual bubbles under initial values of γ of (a) γ = 1.25, (b) γ = 1.70, (c) γ = 2.00, (d) γ = 2.30, (e) γ = 2.80 and (f) γ = 3.25 in an ultrasonic field with a frequency of 20.47 kHz. The initial bubble radius is R_0 = 32 μm.

power was controlled at approximately 53 W.

The evolution cycle of a cavitation bubble is very short. To observe the process of cavitation bubble dynamics, a high speed microphotography system must be adopted. The system consisted of a high speed camera, microscopic optical path, and a light source, as shown in Fig. 1. In the experiment, a Fastcam SA-Z2 high-speed camera (Photron Inc., Japan; the highest acquisition rate was 900,000 fps) was used. Owing to the extremely small size of the transient cavitation bubble (at the millimeter level), we used an inverted fluorescence microscope (Axio Observer A1, Zeiss, Germany) as the microscopic optical path together with the high-speed camera. In addition, a cold light source (100 W) was used to lighten the shooting area during the experiment.

To accurately record the temporal evolution of the first generated bubble in an ultrasonic field, the synchronous control technique was applied to adjust the start times of the three parts of the experimental system, namely, the bubble generation apparatus, the ultrasonic generator system and the high speed microphotography system. The method for synchronously controlling the whole experimental system was implemented on a synchronous control system which consisted of a computer and a synchronizer through two transistor-transistor logic (TTL) signals, which were used to trigger the syringe pump, the

ultrasonic generator and the high-speed camera, as illustrated in Fig. 1. The syringe pump was triggered by the TTL signal 1 to generate a bubble. After a time delay (Δt), when the first generated bubble reached the imaging plane of the microscope, the high-speed camera and the ultrasonic generator were synchronously triggered by the TTL signal 2.

3. Result and discussion

In this section, experiments under various initial conditions are presented to illustrate the temporal evolution of the shape of an individual bubble near a rigid wall. Meanwhile, the time of bubble collapse and the characteristics of the liquid jet are quantified and analyzed.

3.1. Temporal evolution of the bubble shape for various values of γ and R_0

3.1.1. Effects of γ on the temporal evolution of the bubble shape

First, we investigated a single bubble's temporal evolution near a rigid wall at various standoff distances in an ultrasound field with an electric power of 53 W. In these experiments, a single bubble with an initial radius of R_0 = 32 μm was generated near a rigid wall at a wide
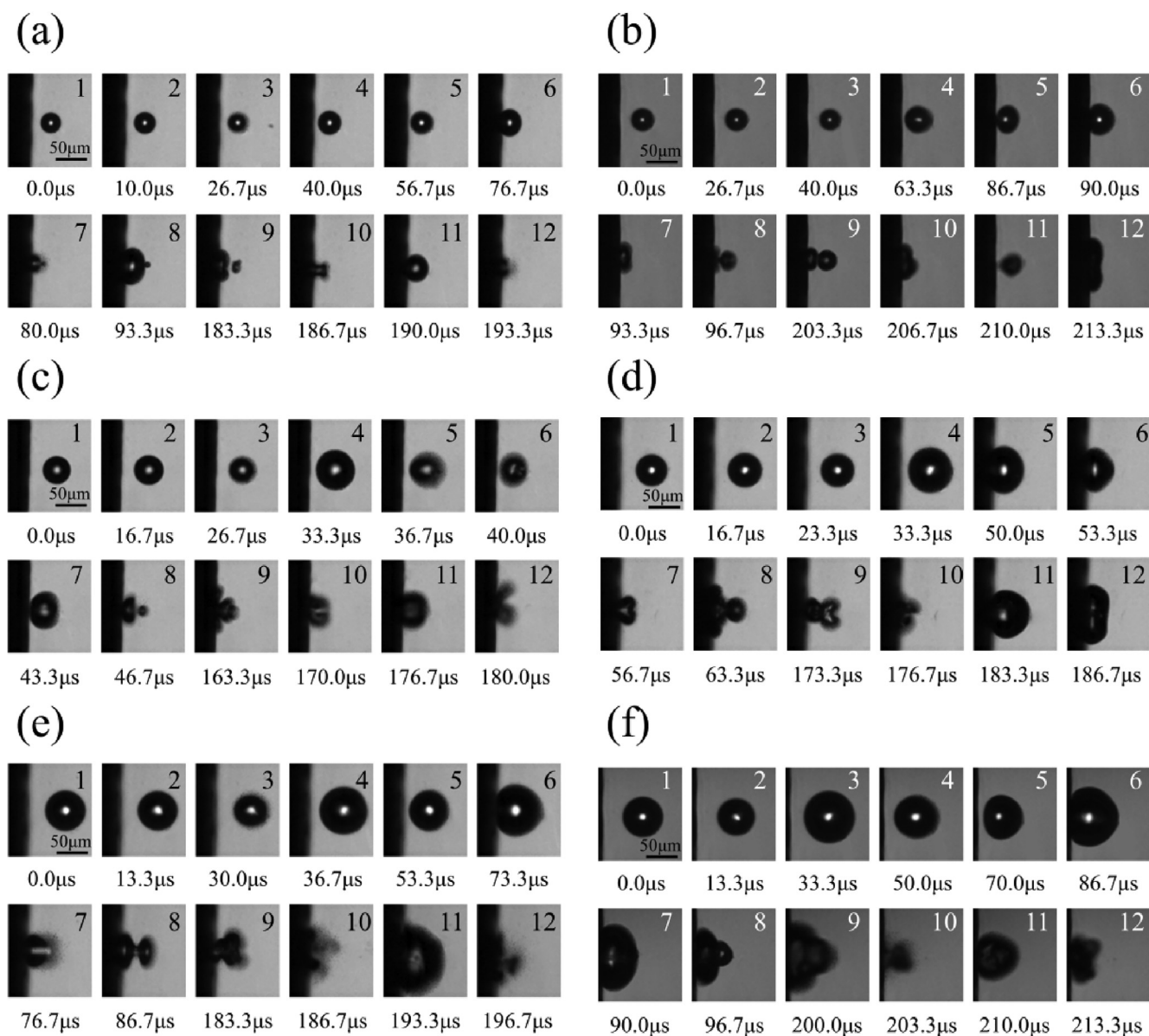
Fig. 6. Comparison of the bubble dynamic behaviors with six initial radii of (a) $R_0 = 18$ μm, (b) $R_0 = 21$ μm, (c) $R_0 = 25$ μm, (d) $R_0 = 28$ μm, (e) $R_0 = 32$ μm and (f) $R_0 = 36$ μm for $\gamma = 2.00$.

range of values of the normalized standoff distance γ, namely, from 1.25 to 3.25. Fig. 5(a–f) shows twelve images from a representative sequence that describe the temporal evolution of bubble shape under various values of γ. The elapsed time t for each frame was calculated from the start of the ultrasound and is specified in microseconds below each frame.

As described in our previous work [37], an individual bubble near a rigid wall goes through four stages (oscillation, movement, collapse and rebound) under ultrasonic wave excitation. As shown in Fig. 5(a–d), when the value of γ varies between 1.25 and 2.30, the single bubble behaviors are similar to the typical dynamic behaviors of the bubble that was discussed in our previous work. The bubble oscillates, moves to the rigid wall, collapses, rebounds and collapses again in a low-frequency ultrasonic field. However, when the standoff distance is small ($\gamma = 1.25$), the collapse process is clearly recorded due to the liquid jet's low velocity (t = 90 μs and 93.3 μs in Fig. 5(a)). As the value of γ increases to 2.80 and 3.25, the dynamic behaviors of the bubble become more similar to those of a bubble in a free field, which have been experimentally investigated by Versluis et al. [8]. The bubble becomes

shape-unstable far from the rigid wall and do not come into direct contact with the solid wall, as shown in Fig. 5(e, f). Under a large value of γ, the high-speed jet does not play a leading role in exerting pressure on the solid wall [39]. Therefore, a single bubble at a large standoff distance has little effects on destructive erosion or other application of acoustic cavitation.

In the present work, we mainly focus on the fierce dynamics of a single acoustic cavitation bubble near a rigid wall. Information on these dynamics would facilitate the elucidation of the mechanism of the high pressure on the nearby wall. Hence, the dynamics of a bubble under three typical normalized standoff distances ($\gamma = 1.70$, 2.00 and 2.30) were investigated with various initial bubble radii and the results will be described in the next section.

3.1.2. Influences of R_0 on the temporal evolution of the bubble shape

In this section, single bubbles with various initial radii that are in the range of 18–36 μm were generated near the rigid wall under three values of γ (1.70, 2.00 and 2.30) and their temporal evolutions in the ultrasonic field with an electric power of 53 W were recorded and
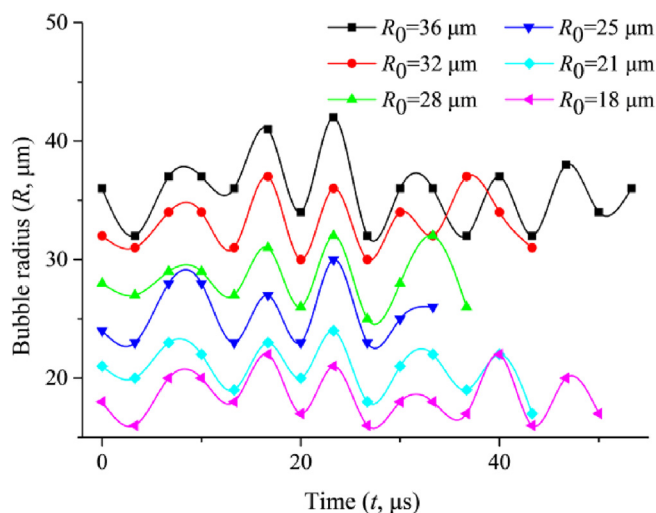
Fig. 7. Temporal evolution of the bubble radius with various values of R_0 for $\gamma = 2.00$.

Fig. 9. Time of bubble collapse as a function of the initial bubble radius R_0 for $\gamma = 1.70$, 2.00 and 2.30.

analyzed. To demonstrate the temporal evolution of the bubble shape, Fig. 6 from (a) to (f) present high-speed photographic records of bubble behaviors near the rigid wall with various initial radii under the typical value of $\gamma = 2.00$. The typical images are chosen to illustrate the essential and pronounced features of the bubble dynamics on the temporal and spatial scales for various values of the initial radius R_0 at a recording rate of 300,000 fps. The elapsed time t for each frame is specified in microseconds below each frame. The time zero ($t = 0$) is defined as the moment that the ultrasonic generator is triggered to operate.

As shown in Fig. 6, bubbles with various initial radii behave similarly near a rigid wall under a typical value of γ (2.00) in an ultrasonic field. Each bubble initially oscillates on site and remain spherical, as shown in frames 1–3 of Fig. 6(a–f). After several cycles, the bubble begins to move toward the rigid wall, as shown in frames 4–6 of Fig. 6(a–f). Then, the bubble collapses with a liquid jet pointing to the rigid wall (frame 7 of Fig. 6(a–f)) and rebounds immediately with a separated small bubble (frame 8 of Fig. 6(a–f)). After rebounding, the separated small bubble collapses and generates a liquid jet that pierces the other bubble and impacts the solid wall (frames 9–10 of Fig. 6(a–f)). Last, the bubble expands and collapses again, as shown in frames 11–12 of Fig. 6(a–f). Meanwhile, the bubble shows similar dynamic behaviors under another two typical values of γ (1.70 and 2.30) (see Fig. S1 and
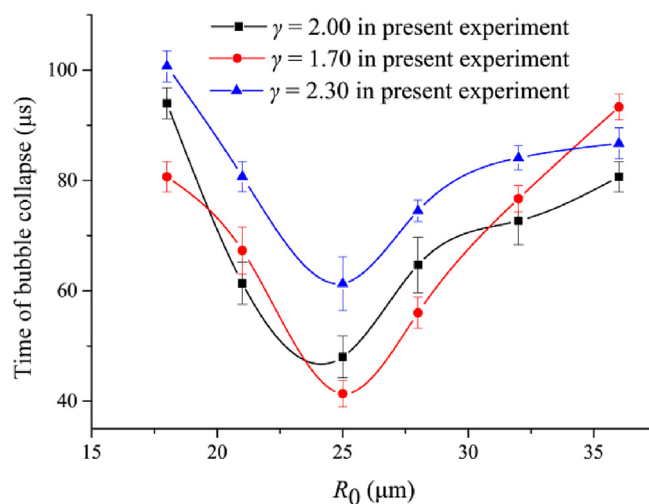
Table 1
The occurrence time of the first three liquid jets under various initial conditions.

R_0 (μm)		18	21	25	28	32	36
γ							
1.70	1st jet	93.3 μs	60 μs	46.7 μs	63.3 μs	73.3 μs	80 μs
	2nd jet	203.3 μs	173.3 μs	166.7 μs	170.0 μs	186.7 μs	190.0 μs
	3rd jet	213.3 μs	186.7 μs	176.7 μs	183.3 μs	196.7 μs	203.3 μs
2.00	1st jet	80 μs	66.7 μs	43.3 μs	56.7 μs	76.7 μs	93.3 μs
	2nd jet	186.7 μs	206.7 μs	170.0 μs	176.7 μs	186.7 μs	203.3 μs
	3rd jet	193.3 μs	213.3 μs	180.0 μs	186.7 μs	196.7 μs	213.3 μs
2.30	1st jet	100 μs	80 μs	60 μs	73.3 μs	83.3 μs	86.7 μs
	2nd jet	206.7 μs	176.7 μs	166.7 μs	176.7 μs	186.7 μs	186.7 μs
	3rd jet	216.7 μs	193.3 μs	173.3 μs	183.3 μs	193.3 μs	196.7 μs

Fig. S2 in the Supplementary material).

To illustrate the oscillation properties of the acoustic bubble during the first several cycles, the bubble radius at every time point during oscillation was calculated and is presented in Fig. 7 for $\gamma = 2.00$. Although the initial values of the bubble radius differ, the bubble oscillates regularly with the same frequency of approximately 120 kHz, which results from the combined action of the ultrasonic field, the higher harmonic and the nearby solid wall. As a result, the bubble near the rigid wall in the ultrasonic field is forced to oscillate with a
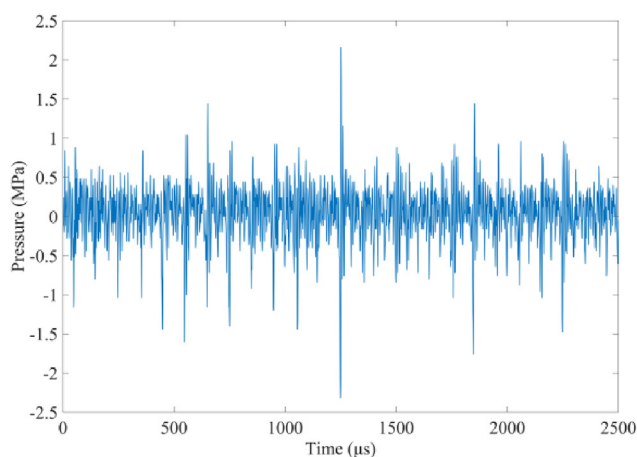
(a)
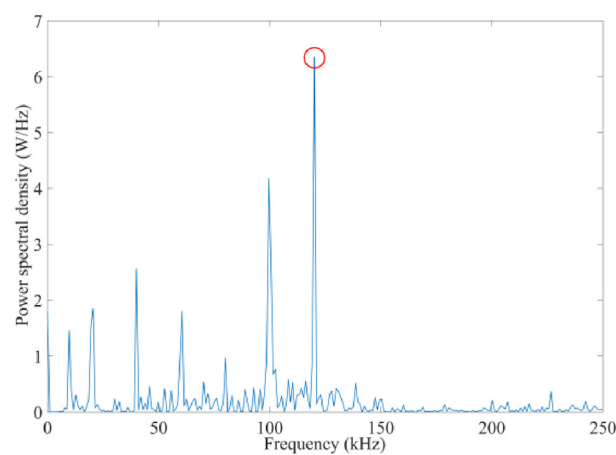
(b)

Fig. 8. (a) Pressure-time profile that was recorded by the hydrophone near the rigid wall and (b) the corresponding frequency spectrum graph.
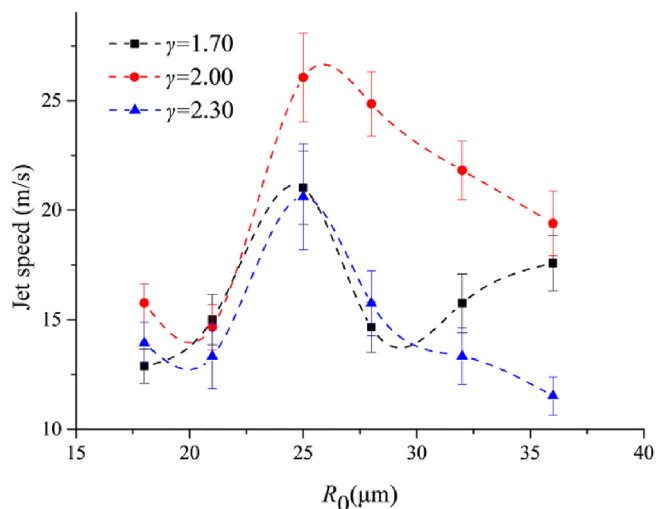
Fig. 10. The speed of the first liquid jet as a function of the initial bubble radius R_0 for $\gamma = 1.70$, 2.00 and 2.30.

frequency of approximately 120 kHz in these experiments. To further illustrate the frequency characteristics of the driving force near the rigid wall in the ultrasonic field, a hydrophone (TC4013, RESON, Denmark) was placed near the rigid wall to measure the pressure in the liquid, as shown in Fig. 8(a). After processing the pressure data via Fourier transform, the corresponding frequency spectrum graph was obtained, as shown in Fig. 8(b). The highest peak occurs at approximately 120 kHz, which accords with the bubble oscillation frequency.

3.2. Time of bubble collapse

The time of bubble collapse in an ultrasonic field (t_{COL}) is defined as the length of time interval between time zero ($t = 0$) and the first collapse of the bubble. As the high-speed jets that are emitted during collapse have substantial effects on destructive erosion or surface cleaning, the time of bubble collapse is regarded as an important characteristic of acoustic cavitation [12]. To further investigate the characteristics of the acoustic cavitation bubble's behaviors under various initial conditions, t_{COL} was calculated.

As shown in Fig. 9, the time of bubble collapse t_{COL} changes with the bubble's initial radius and shows a similar trend, which resembles a

valley, under various standoff distances, and the error bar of each point is relatively low. When the initial radius of the bubble R_0 increases from 18 μm to 25 μm, the value of t_{COL} decreases substantially. Then, the value of t_{COL} increases as R_0 further increases from 25 μm to 36 μm. As a result, there are three minimum values of t_{COL} under the three typical values of γ (1.70, 2.00 and 2.30) when the bubble's initial radius R_0 is approximately 25 μm. As reported by Leighton [40], the natural frequency f of an acoustically oscillated spherical bubble can be approximated by small amplitude behavior of Rayleigh–Plesset equation,

$$f^2 = \frac{1}{4\rho\pi^2 a^2}\left\{3\kappa\left(P_0 + \frac{2\sigma}{a}\right) - \frac{2\sigma}{a}\right\}, \tag{1}$$

where ρ is the density of the fluid (1,000 kg·m^{-3}), σ is the surface tension of water (0.0728 N·m^{-1}), κ is the polytropic exponent (1.4) for a bubble that contain air, P_0 is the hydrostatic liquid pressure (101325 Pa), and a is the radius of the bubble at an equilibrium state. For a bubble with $R_0 = 25$ μm, the natural frequency is calculated to be 123 kHz, which is almost equal to the frequency of the force around the bubble in the liquid (approximately 120 kHz), which has been discussed in the previous section, as shown in Fig. 8. Thus, the bubble with $R_0 = 25$ μm fully expands to a higher multiple of volume compared to its initial value (as shown in frame 4 of Fig. 6(c)) and collapses fiercely. That could be the main reason that the bubble with $R_0 = 25$ μm collapsed earliest in our experiments.

In addition, the bubble always collapses later when the value of γ is 1.70 or 2.30 and collapses earliest when $\gamma = 2.00$. This is mainly due to the influence of the rigid wall. Under a small value of γ ($\gamma = 1.70$), the expanse of the bubble is confined by the rigid wall during the oscillation of the bubble and the bubble oscillates for more cycles prior to collapse (see Fig. S1 in the Supplementary material). In contrast, the influence of the rigid wall is weak for a relatively large value of γ (2.30), which causes the bubble to move to the rigid wall slower and to collapse later (see Fig. S2 in the Supplementary material).

3.3. Jet characteristics

The liquid jet that formed during the collapse phase of the bubble is considered as an important factor that contributes to destructive erosion or surface cleaning. To further analyze the dynamics of the bubble in detail, the velocities of the liquid jet in the direction of the rigid wall were calculated, which were determined from a photographic series with 300, 000 frames per second, namely, the average velocity of the jet is calculated over a time interval of 3.3 μs. Meanwhile, more than one
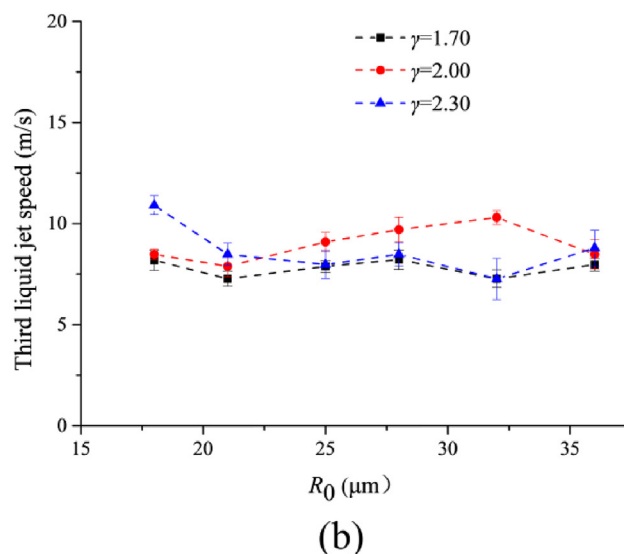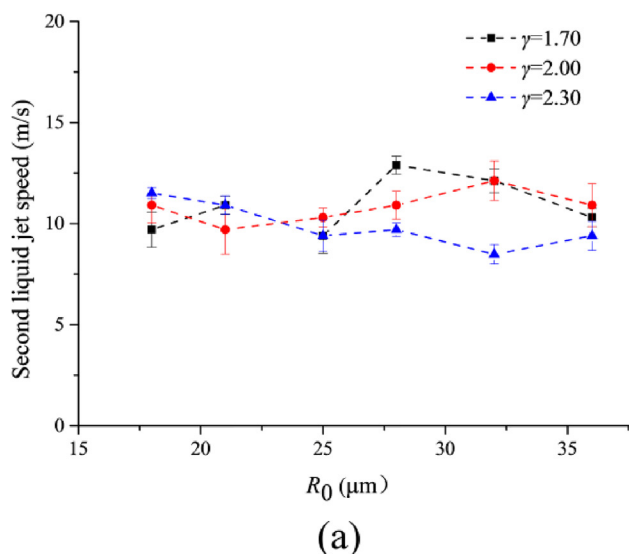

(a)

(b)

Fig. 11. The speeds of (a) the second liquid jet and (b) the third liquid jet as functions of the initial radius of bubble R_0 for $\gamma = 1.70$, 2.00 and 2.30.

liquid jet forms when the bubble is under the excitation of the ultrasonic field. In this part, the occurrence times and the velocities of the first three liquid jets were recorded and analyzed.

The occurrence times of the first three liquid jets are listed in Table 1. The occurrence time of the first liquid jet, which corresponds to the time of bubble collapse, has been analyzed in Section 3.2. According to Table 1, the intervals between adjacent liquid jets are almost constant under various initial conditions. Furthermore, to better illustrate the differences in the liquid jets' velocities under three typical values of γ and various initial radii of bubble R_0, figures are presented in Figs. 10 and 11.

According to Fig. 10, the error bars are relatively large because of the higher speed of the first liquid jet and the limitation of the temporal resolution in the experiments, but there are still substantial changes in the velocity of the first liquid jet (v_1) under various initial conditions. First, the peak value of the first liquid jet's velocity (v_1) is attained when the initial radius of the bubble is approximately 25 μm under all three typical values of γ. The peak value ranges from 20.61 to 26.06 m/s. Second, the liquid jets that are ejected when $\gamma = 2.00$ have higher velocities than those under the other two typical values of γ (1.70 and 2.30). These results accord with the results of the time of bubble collapse, and an explanation of these results has been provided in the previous section.

However, the velocities of the second and third liquid jets show no obvious variation trends under various initial conditions, and the short error bars indicate high precision of the measurement, as shown in Fig. 11. After collapse, the bubbles that are touching the rigid wall under various initial conditions exhibit similar behaviors; hence, the initial conditions have less influence on the bubble dynamics after the collapse phase.

4. Conclusions

Experimental studies are presented in which the effects of the normalized standoff distance and the initial bubble radius on the dynamics of a bubble near a rigid wall in an ultrasonic field are investigated. High-speed videos of bubble evolution are recorded for investigating the bubble outline and the formation of liquid jets. Statistics on the bubble collapse time and the velocities of the liquid jets are also presented to quantify the dynamic behaviors of the bubble. The main conclusions and new findings in present work are summarized as follows:

1. The bubble shape variation, which includes oscillation, movement, jet formation and rebound of the bubbles, differs within a range of normalized standoff distances γ from 1.25 to 2.30. A collapsed bubble with a value of γ in the range of 1.70–2.30 in an ultrasonic field typically induces high-speed liquid jets that point to the nearby rigid wall, which play an important role in destructive erosion and surface cleaning.

2. The initial radius of the bubble strongly influences the time of the bubble collapse and the velocity of the first liquid jet under three typical values of γ (1.70, 2.00 and 2.30). When the value of R_0 ranges from 18 to 36 μm, a valley value of t_{COL} and a peak value of v_1 are attained when the initial radius of the bubble is approximately 25 μm. Hence, a bubble with the optimal initial size collapses the most fiercely and contributes most to the applications of acoustic cavitation, such as destructive erosion and surface cleaning. The optimal initial radius of the bubble is 25 μm in present experiments.

3. Among the three typical values of γ (1.70, 2.00 and 2.30), the dynamic behaviors of the bubble in the ultrasonic field are the fiercest for $\gamma = 2.00$. For $\gamma = 2.00$, the bubble collapses earlier with a higher speed of the first liquid jet compared to the other two typical values of γ that are considered in the present work.

4. After rebounding, the bubble near a rigid wall in the ultrasonic field collapses with a liquid jet more than once. The time interval between two adjacent liquid jets is almost constant among initial conditions. In addition, the velocities of the second and the third liquid jets show no obvious variation trends as the initial conditions change.

5. In summary, the initial radius of the bubble and the value of γ both strongly affect the dynamic behaviors of a bubble in a low-frequency ultrasonic field, which are the main mechanism of most applications of acoustic cavitation. Under suitable initial conditions ($R_0 = 25$ μm and $\gamma = 2.00$ in the present experiment), the bubble collapses fiercely earlier with higher speed liquid jets compared to other initial conditions. These results demonstrate how the initial bubble radius and the standoff distance affect the bubble dynamics and can be used to facilitate exploration of the mechanism of acoustic cavitation.

CRediT authorship contribution statement

Hao Wu: Conceptualization, Methodology, Data curation, Writing - original draft, Investigation. **Cheng Zhou:** Visualization, Formal analysis, Software. **Zhihua Pu:** Software, Validation. **Xiaochen Lai:** Visualization. **Haixia Yu:** Supervision, Writing - review & editing. **Dachao Li:** Supervision, Funding acquisition.

Declaration of Competing Interest

The authors declare that they have no known competing financial interests or personal relationships that could have appeared to influence the work reported in this paper.

Acknowledgements

Appendix A. Supplementary data

Supplementary data to this article can be found online at https://doi.org/10.1016/j.ultsonch.2020.105197.

References

[1] G.L. Chahine, A. Kapahi, J.K. Choi, C.T. Hsiao, Modeling of surface cleaning by cavitation bubble dynamics and collapse, Ultrason. Sonochem. 29 (2016) 528–549.

[2] F. Reuter, R. Mettin, Mechanisms of single bubble cleaning, Ultrason. Sonochem. 29 (2016) 550–562.

[3] F. Reuter, S. Lauterborn, R. Mettin, W. Lauterborn, Membrane cleaning with ultrasonically driven bubbles, Ultrason. Sonochem. 37 (2017) 542–560.

[4] T. Leong, P. Juliano, K. Knoerzer, Advances in ultrasonic and megasonic processing of foods, Food Eng. Rev. 9 (2017) 237–256.

[5] W. Eisenmenger, The mechanisms of stone fragmentation in ESWL, Ultrasound Med. Biol. 27 (2001) 683–693.

[6] G.A. Curtiss, D.M. Leppinen, Q.X. Wang, J.R. Blake, Ultrasonic cavitation near a tissue layer, J. Fluid Mech. 730 (2013) 245–272.

[7] X.J. Ma, T.Y. Xing, B. Huang, Q.H. Li, Y.F. Yang, Combined experimental and theoretical investigation of the gas bubble motion in an acoustic field, Ultrason. Sonochem. 40 (2018) 480–487.

[8] M. Versluis, D.E. Goertz, P. Palanchon, I.L. Heitman, S.M. van der Meer, B. Dollet, N. de Jong, D. Lohse, Microbubble shape oscillations excited through ultrasonic parametric driving, Phys. Rev. E 82 (2010).

[9] M. Ashokkumar, The characterization of acoustic cavitation bubbles - an overview, Ultrason. Sonochem. 18 (2011) 864–872.

[10] C.E. Brennen, Cavitation and Bubble Dynamics, Oxford University Press, New York, 1995.

[11] M. Kornfeld, L. Suvorov, On the destructive action of cavitation, J. Appl. Phys. 15 (1944) 495–506.

[12] X.J. Ma, B.A. Huang, X. Zhao, Y. Wang, Q. Chang, S.C. Qiu, X.Y. Fu, G.Y. Wang, Comparisons of spark-charge bubble dynamics near the elastic and rigid boundaries, Ultrason. Sonochem. 43 (2018) 80–90.

[13] Q.X. Wang, K. Manmi, Three dimensional microbubble dynamics near a wall subject

to high intensity ultrasound, Phys. Fluids 26 (2014) 032104.

[14] S. Merouani, O. Hamdaoui, Y. Rezgui, M. Guemini, Theoretical estimation of the temperature and pressure within collapsing acoustical bubbles, Ultrason. Sonochem. 21 (2014) 53–59.

[15] M.L. Calvisi, O. Lindau, J.R. Blake, A.J. Szeri, Shape stability and violent collapse of microbubbles in acoustic traveling waves, Phys. Fluids 19 (2007) 047101.

[16] Y.Q. Liu, K. Sugiyama, S. Takagi, Y. Matsumoto, Numerical study on the shape oscillation of an encapsulated microbubble in ultrasound field, Phys. Fluids 23 (2011) 041904.

[17] X.J. Ma, B.A. Huang, Y.K. Li, Q. Chang, S.C. Qiu, Z. Su, X.Y. Fu, G.Y. Wang, Numerical simulation of single bubble dynamics under acoustic travelling waves, Ultrason. Sonochem. 42 (2018) 619–630.

[18] G. Servant, J.P. Caltagirone, A. Gerard, J.L. Laborde, A. Hita, Numerical simulation of cavitation bubble dynamics induced by ultrasound waves in a high frequency reactor, Ultrason. Sonochem. 7 (2000) 217–227.

[19] A. Osterman, M. Dular, B. Sirok, Numerical simulation of a near-wall bubble collapse in an ultrasonic field, J. Fluid Sci. Technol. 4 (2009) 210–221.

[20] B. Boyd, S. Becker, Numerical modelling of an acoustically-driven bubble collapse near a solid boundary, Fluid Dyn. Res. 50 (2018).

[21] S.P. Wang, Q.X. Wang, D.M. Leppinen, A.M. Zhang, Y.L. Liu, Acoustic bubble dynamics in a microvessel surrounded by elastic material, Phys. Fluids 30 (2018).

[22] X. Ye, X.L. Yao, L.Q. Sun, B. Wang, Cavitation bubble in compressible fluid near the rigid wall subjected to the acoustic wave with arbitrary incidence angle in three-dimensional, J. Mech. 31 (2015) 307–318.

[23] A.M. Zhang, S.P. Wang, G.X. Wu, Simulation of bubble motion in a compressible liquid based on the three dimensional wave equation, Eng. Anal. Bound Elem. 37 (2013) 1179–1188.

[24] G.L. Chahine, K.M. Kalumuck, BEM software for free surface flow simulation including fluid-structure interaction effects, Int. J. Comput. Appl. T 11 (1998) 177–198.

[25] Z.Y. Wang, Y.K. Li, B. Huang, D.M. Gao, Numerical investigation on the influence of surface tension and viscous force on the bubble dynamics with a CLSVOF method, J. Mech. Sci. Technol. 30 (2016) 2547–2556.

[26] Q.X. Wang, J.R. Blake, Non-spherical bubble dynamics in a compressible liquid. Part 1. Travelling acoustic wave, J. Fluid Mech. 659 (2010) 191–224.

[27] Q.X. Wang, J.R. Blake, Non-spherical bubble dynamics in a compressible liquid. Part 2. Acoustic standing wave, J. Fluid Mech. 679 (2011) 559–581.

[28] S.W. Ohl, E. Klaseboer, B.C. Khoo, Bubbles with shock waves and ultrasound: a review, Interface Focus 5 (2015).

[29] T.G. Leighton, Bubble population phenomena in acoustic cavitation, Ultrason. Sonochem. 2 (1995) S123–S136.

[30] J.R. Blake, G.S. Keen, R.P. Tong, M. Wilson, Acoustic cavitation: the fluid dynamics of non-spherical bubbles, Philos. T R Soc. A 357 (1999) 251–267.

[31] N. Vyas, H. Dehghani, R.L. Sammons, Q.X. Wang, D.M. Leppinen, A.D. Walmsley, Imaging and analysis of individual cavitation microbubbles around dental ultrasonic scalers, Ultrasonics 81 (2017) 66–72.

[32] R.E.A. Arndt, Cavitation in vortical flows, Annu. Rev. Fluid Mech. 34 (2002) 143–175.

[33] F.S. Bai, K.A. Saalbach, J. Twiefel, J. Wallaschek, Effect of different standoff distance and driving current on transducer during ultrasonic cavitation peening, Sens. Actuat. A-Phys. 261 (2017) 274–279.

[34] W. Kim, K. Park, J. Oh, J. Choi, H.-Y. Kim, Visualization and minimization of disruptive bubble behavior in ultrasonic field, Ultrasonics 50 (2010) 798–802.

[35] W. Lauterborn, H. Bolle, Experimental investigations of cavitation-bubble collapse in the neighbourhood of a solid boundary, J. Fluid Mech. 72 (2006) 391–399.

[36] E.A. Brujan, Cavitation bubble dynamics in non-Newtonian fluids, Polym. Eng. Sci. 49 (2009) 419–431.

[37] H. Wu, C. Zhou, Z. Pu, H. Yu, D. Li, Effect of low-frequency ultrasonic field at different power on the dynamics of a single bubble near a rigid wall, Ultrason. Sonochem. 104704 (2019).

[38] P. Palanchon, J. Klein, N. de Jong, Production of standardized air bubbles: application to embolism studies, Rev. Sci. Instrum. 74 (2003) 2558–2563.

[39] S. Li, R. Han, A.M. Zhang, Q.X. Wang, Analysis of pressure field generated by a collapsing bubble, Ocean Eng. 117 (2016) 22–38.

[40] T.G. Leighton, The Acoustic Bubble, Academic London, 1994.